ACS OMEGA

Open Access

http://pubs.acs.org/journal/acsodf

Article

Surface Modification of ZnO Nanotubes by Ag and Au Coatings of Variable Thickness: Systematic Analysis of the Factors Leading to UV Light Emission Enhancement

Maksymilian Włodarski, Michał P. Nowak, Matti Putkonen, Piotr Nyga, and Małgorzata Norek*

Cite This: *ACS Omega* 2024, 9, 1670−1682

Read Online

ACCESS | Metrics & More | Article Recommendations | Supporting Information

ABSTRACT: Surface modification by plasmonic metals is one of the most promising ways to increase the band-to-band excitonic recombination in zinc oxide (ZnO) nanostructures. However, the metal-induced modulation of the UV light emission depends strongly on the production method, making it difficult to recognize the mechanism responsible for charge/energy transfer between the semiconductor and a metal. Therefore, in this study, the ZnO/Ag and Au hybrids were produced by the same, fully controlled experimental approach. ZnO nanotubes (NTs), fabricated by a template-assisted ALD synthesis, were coated by metals of variable mass thickness (1−6.5 nm thick) using the electron beam PVD technique. The deposited Ag and Au metals grew in the form of island films made of metallic nanoparticles (NPs). The size of the NPs and their size distribution decreased, while the spacing between the NPs increased as the mass of the deposited Ag and Au metals decreased. Systematic optical analysis allowed us to unravel a specific role of surface defects in ZnO NTs in the processes occurring at the ZnO/metal interface. The enhancement of the UV emission was observed only in the ZnO/Ag system. The phenomena were tentatively ascribed to the coupling between the defect-related (DL) excitonic recombination in ZnO and the localized surface plasmon resonance (LSPR) at the Ag NPs. However, the enhancement of UV light was observed only for a narrow range of Ag NP dimensions, indicating the great importance of the size and internanoparticle spacing in the plasmonic coupling. Moreover, the enhancement factors were much stronger in ZnO NTs characterized by robust DL-related emission before metal deposition. In contrast to Ag, Au coatings caused quenching of the UV emission from ZnO NTs, which was attributed to the uncoupling between the DL and LSP energies in this system and a possible formation of the ohmic contact between the Au metal and the ZnO.

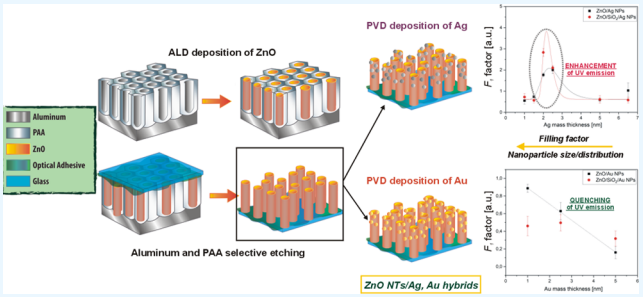

1. INTRODUCTION

Zinc oxide (ZnO) is considered a prospective candidate that can substitute gallium nitride (GaN)-based materials in the mass production of various optoelectronic devices, such as efficient ultraviolet (UV) light-emitting devices (LEDs) or low threshold UV lasers.[1−3] ZnO possesses similar physical properties to GaN, such as a wide direct band gap (3.37 eV) and the same wurtzite structure with a small lattice mismatch on the *c*-plane (∼1.8%). Apart from that, ZnO has many advantages over GaN, including a larger exciton binding energy (60 meV) as compared to that of GaN (25 meV) and a lower refractive index than that of GaN (2.0 versus 2.4 at 587.6 nm). The larger excitonic binding energy translates into a greater external quantum efficiency that can lead to intense exciton emission of light at the band edge even at (or above) room temperature. The lower refractive index contributes to a greater light extraction efficiency from the ZnO emitter. Furthermore, various nanostructure forms of ZnO crystals can be produced by a large variety of inexpensive chemical protocols.[3] In addition, ZnO is environmentally friendly and chemically stable.

Yet, the generation of intensive UV light from ZnO material remains problematic due to the presence of deep and shallow defect states within the band gap that hinder the transition of electrons from the conduction band (CB) to the valence band (VB) (band-to-band recombination). There are several approaches to circumvent this problem.[4] The use of plasmonic metals stands out among them as the most promising method to deactivate the defects and enhance UV light. Metallic nanoparticles (NPs) that can sustain the localized surface plasmons (LSPs) scatter incident light and locally amplify the electromagnetic fields.[5−7] This concentrated energy can be

Received: October 20, 2023
Revised: December 7, 2023
Accepted: December 11, 2023
Published: December 27, 2023

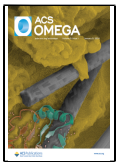

harnessed to increase exciton density at ZnO, providing that there is a match between the exciton recombination energy in the semiconductor and the electron oscillation of surface plasmons (SPs) at the metal/semiconductor interface.[8,9]

This simple idea of causing the NBE emission enhancement seems to be quite complicated to put in practice. Most of the research done so far concentrated around silver (Ag) and gold (Au) nanoparticles, owing to their excellent scattering properties that provide intensive and well-resolved resonances and a good stability.[10−12] Despite the fact that heat LSP resonances (LSPRs) generated by Ag and Au do not match with the band-to-band transition energy in ZnO, the metals contributed to a significant amplification of the NBE emission.[13−16] Different mechanisms were proposed to explain the observed enhancement. In ZnO/Au hybrid systems, the UV enhancement was often attributed to the coupling between defect-related (DL) emission in ZnO and LSPR at the metal and to the LSPR-assisted electron transfer from Au NPs to the conduction band of ZnO.[17−24] Plasmon-mediated NBE enhancement was also observed in ZnO/Ag NP systems.[15,25−2627] The better optical performance was frequently attributed to favorable energy band alignments in these systems,[28,29,15] or to the excitation of the SPs by the ZnO DL emission band (via the DL-LSP coupling), and the resulting local field enhancement effect inducing increased excitonic recombination rate.[9,26,30] In these works, the role of defect density was highlighted and considered as an indispensable condition for the Ag and Au plasmon-mediated enhancements to occur. Other works, however, suggested that the presence of the defect band in PL spectra is actually not necessary to enhance the luminescence in ZnO.[31,32] According to the latter works, the enhancement occurs via a surface energy (nonradiative)-transfer mechanism that involves the ZnO exciton coupling to intra- or interband transitions in the metal. The extra energy that is gained by the electrons at the metal makes it possible for them to overcome the metal−semiconductor contact barrier and be injected into the CB in ZnO.

It should be noted that in the above works the enhancement factors in the ZnO/Ag and ZnO/Au systems varied significantly (from a few to several dozen). Moreover, quenching of NBE luminescence in ZnO upon the introduction of Ag or Au NPs was also reported.[33−37] Although it is not entirely clear what causes this state of affairs, these inconsistencies were most likely due to the different experimental conditions used to prepare the hybrids and the resulting different material configurations, which led to different optical parameters of the systems. For instance, the ZnO wires with micrometer scale diameter showed smaller enhancement compared to those with nanometer-scale diameter.[14] Depending on the technique used to deposit Au, UV emission was enhanced (dc sputtering) or quenched (thermal evaporation).[38] Similar results were presented by Purahmad et al.[39] who observed a strong enhancement of the NBE band from ZnO NWs when Al and Ni NPs were deposited by radiofrequency magnetron sputtering and a quenching of the UV band intensity when the NPs were deposited by e-beam evaporation. Therefore, to enable a reliable comparison of the effects caused by the Ag and Au metals themselves without the influence of external experimental variables, the same protocol for the preparation of the ZnO/Ag and ZnO/Au hybrid systems should be used. The comparison in such circumstances should allow, in turn, the proper recognition of differences and similarities between the processes at the ZnO/Ag and ZnO/Au interfaces induced by these metals.

In this work, we study the photoluminescence (PL) performance of ZnO nanotubes (NTs) fabricated by template-assisted ALD synthesis. The PL was modified by Ag and Au island films deposited on the ZnO NT surface by using electron beam evaporation. Systematic optical analysis of the changes induced by plasmonic metals in the fully controlled ZnO/Ag, Au systems allowed us to identify the factors responsible for the UV light emission enhancement. This approach provided new insights into the role of defect density in ZnO, metal particle size and spacing, and the strength of plasmonic coupling in the NBE emission enhancement. The data will hopefully contribute to more predictable system development based on ZnO−metal hybrid nanostructures, leading to the production of efficient and cheap UV light emitters.

2. EXPERIMENTAL SECTION

Porous anodic alumina (PAA) templates were synthesized in a two-step anodization of high-purity aluminum foil (99.9995% Al, Puratronic, Alfa-Aesar) using the following conditions in the first step: 0.3 M oxalic acid electrolyte containing a 1:3 v/v ethanol/water mixture, an applied voltage of 160 V, a temperature of 0 °C, and an anodizing time of 2 h. After the process, alumina was chemically removed using a mixture of 6 wt % of phosphoric acid and 1.8 wt % of chromic acid at 60 °C for 120 min. In the second step of anodization, the following electrochemical parameters were applied: 0.2 M phosphoric acid solution, a voltage of 170 V, an electrolyte temperature of 10 °C, and an anodizing time of 20 min.

The ALD depositions of ZnO were performed at 150 °C in a Picosun SUNALE R-150 reactor (Picosun Oy, Espoo, Finland). The operating pressure of the reaction chamber was approximately 10 mbar. Inert nitrogen gas with a purity of 99.999% was used as the carrier and purge gas. Diethyl zinc (DEZ, ≥52 wt % Zn basis, Sigma-Aldrich) and distilled (DI) water were used as precursors for the deposition of ZnO. A pulse time of 0.3 s and a purge time of 10.0 s were used for both precursors. The film thickness was ∼56 nm after 275 deposition cycles, measured from reference Si(100) substrates by ellipsometry (FS-1 Multi-Wavelength Ellipsometer, Film-Sense LLC).

After the ZnO deposition, the samples were fixed on microscope glass substrates using an NOA 63 optical adhesive purchased from the Norland Company. Then, the aluminum substrate was selectively detached from the PAA template using a saturated solution of $HCl/CuCl_2$. Next, the PAA templates were dissolved in a 0.1 M NaOH solution by keeping the samples in the alkaline solution at 42 °C for 40 min.

Island-type Ag and Au films were deposited by the electron beam physical vapor deposition technique (Syrus III 1100, Bühler Leybold Optics) in two steps. First, a silicon dioxide (SiO_2) layer was deposited on top of a part of prepared ZnO nanotube arrays and glass substrates (Umicore). Second, metallic NPs were deposited on the top of ZnO nanotube arrays and glass substrates, with and without SiO_2. Before deposition, both substrates were blown with nitrogen gas and glass was cleaned with ethanol. Both deposition steps were prepared with the following parameters: base pressure better than 3.0×10^{-6} mbar, deposition rates of gold (Au, purity

https://doi.org/10.1021/acsomega.3c08253
ACS Omega 2024, 9, 1670−1682

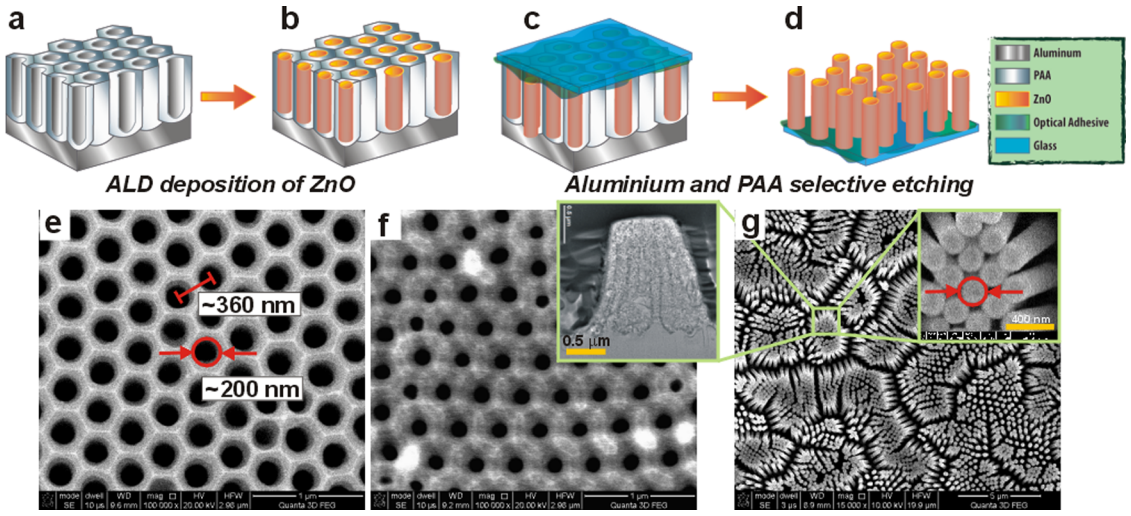

Figure 1. Scheme showing the preparation steps of ZnO NTs: porous anodic alumina (PAA) template on Al substrate (a), PAA on Al substrate after the deposition of ZnO material in the pore interior (b), the sample PAA + ZnO on Al substrate fixed on the glass by the optical adhesive (c), free-standing ZnO NTs on glass after the selective dissolution of Al substrate and PAA template (d), SEM image of a top part of PAA with $D_p \sim$ 200 nm and $D_c \sim$ 360 nm (e), SEM image of a top view of the PAA template after ZnO deposition (f), SEM image of the free-standing ZnO NTs (a top view): the left inset is a TEM image of a cross-sectional view of a bunch of ZnO NTs, whereas the right inset is a larger magnification of the selected area in the SEM image (g).

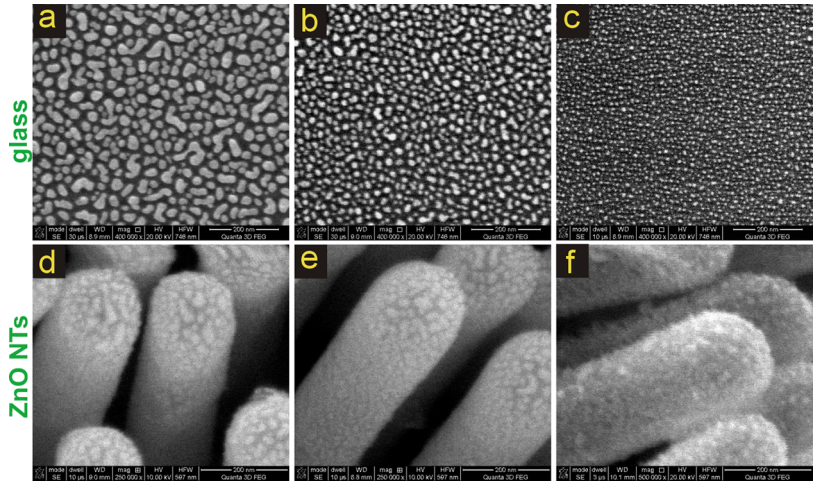

Figure 2. SEM images of Au NPs forming island films deposited on glass (a–c) and on the top of ZnO NTs (d–f) with the nanoparticle size distribution Au NPs-5 (a, d), Au NPs-2.5 (b, e), and Au NPs-1 (c, f), as shown in Figure S1a–c (Supporting Information).

99.99%, Kurt J. Lesker) and silver (Ag, purity 99.99%, Unicore) 0.065 nm/s, and of silicon dioxide (SiO_2, purity 99.99%, Umicore) 0.02 nm/s. The substrate temperature was 35 °C. Mass thickness (corresponding to a hypothetical continuous film) and deposition rates were measured with a quartz crystal microbalance.

X-ray diffraction (XRD) analysis was carried out using a Seifert C3000 diffractometer with Cu Kα radiation at the operating parameters of 30 mA, 50 kV, and a step size of 0.02°/1 s. The morphology of the samples was studied using an FE-SEM (FEI, Quanta) field emission scanning electron microscope equipped with an energy-dispersive X-ray spectrometer (EDS). The microstructure of the samples was analyzed with a high-resolution transmission electron microscope (HR-TEM). The HR-TEM specimens (lamellas) were prepared by focused ion (Ga^+) beam (FIB) using platinum (Pt) as the protective layer. The analyses were performed in a Titan G2 60–300 kV (FEI company) microscope equipped with a field emission gun (FEG) operating at 300 kV. Scanning transmission electron microscopy (STEM) was performed with the use of a high-angle annular dark-field detector (HAADF). Elemental mapping was performed using the STEM–EDX (energy-dispersive X-ray) analysis technique.

Transmittance spectra were measured with a Cary 7000 spectrometer (Agilent), equipped with a 150 mm integration sphere (due to the high scattering nature of the samples). The transmittance spectrum of the glass coated with NOA 63 adhesive was subtracted from the measured spectra.

Photoluminescence (PL) spectra were collected using a Spectra Pro 2150i spectrometer with an ICCD camera (Acton Research Corp.). The samples were excited by a 266 nm laser (Intelite Inc.). To maintain an adequate comparability of the measured fluorescence intensity level between samples, the measurements were always referenced to the UV peak intensity generated by a 1 μm thick GaN layer on a Si substrate (the standard reference sample), measured at the same time as

https://doi.org/10.1021/acsomega.3c08253
ACS Omega 2024, 9, 1670–1682

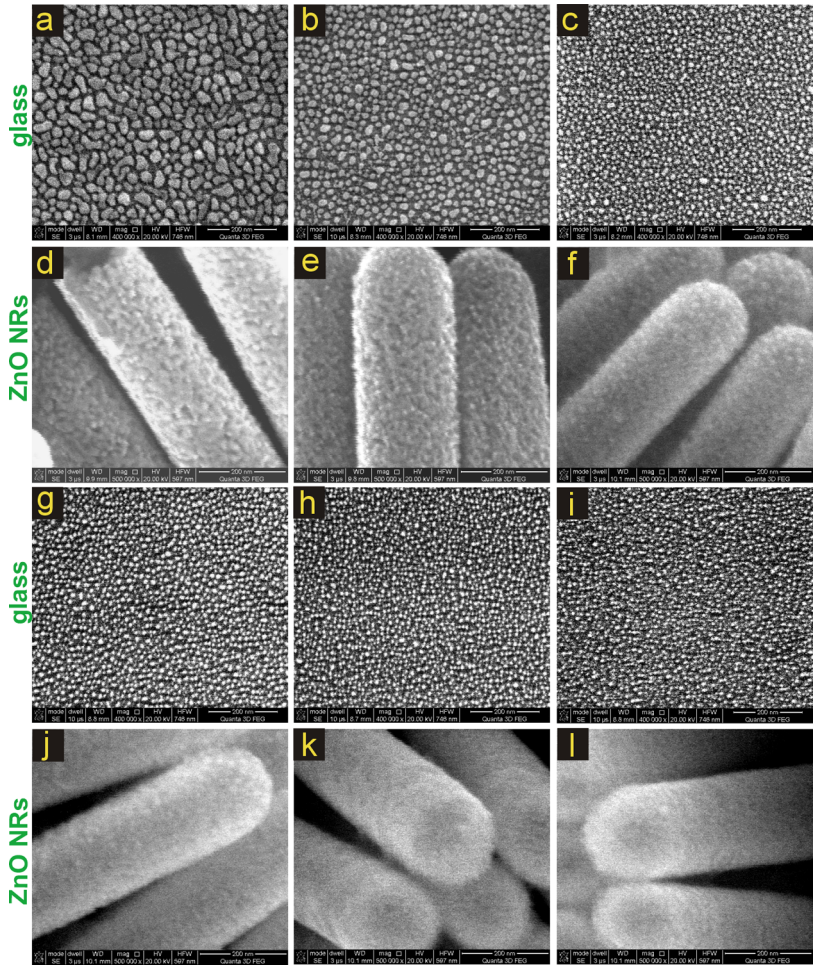

Figure 3. SEM images of Ag NPs forming island films deposited on glass (a–c) and (j–l) and on the top of ZnO NTs (d–f) and (g–i) with the nanoparticle size distribution Ag NPs-6.5 (a, d), Ag NPs-5 (b, e), Ag NPs-2.5 (c, f), Ag NPs-2 (g, j), Ag NPs-1.5 (h, k), and Ag NPs-1 (i, l), as shown in Figure S2a–f (Supporting Information).

samples. The results were then normalized to this reference value.

3. RESULTS AND DISCUSSION

The PAA-assisted synthesis of free-standing ZnO nanotubes using the ALD technique is depicted in Figure 1. The templates with a pore diameter (D_p) and an interpore distance (D_c) of ca. 200 and 360 nm, respectively, were used in the synthesis (Figure 1e). After the ZnO deposition process, the pores in PAA became visibly smaller (Figure 1f). The resulting ZnO NTs inherit the morphology of the PAA template. Closed tips of ZnO nanotubes (the inset in Figure 1g) are due to full coverage of the pore interior, including dome-like pore bottoms, by the ZnO material during ALD deposition. The external diameter and the length of ZnO nanotubes correspond to the D_p and depth of pores in PAA, respectively (insets in Figure 1g). The left inset in Figure 1g shows a cross-sectional view of a bunch of ZnO NTs. Based on the TEM image, the length of the nanotubes can be estimated to be about 2 μm.

Hybrid ZnO–Au, Ag nanostructures were prepared by deposition of the metals on the top of ZnO NT arrays using the PVD technique. In Figure 2, SEM images of Au island films, for different masses (5, 2.5, and 1 nm), deposited on glass (Figure 2a–c) and ZnO NT surfaces (Figure 2d–f) are shown. It can be observed that the shape of nanoparticles changes from rather irregular for larger nanoparticles (Figure 2a) to more spherical for smaller ones (Figure 2b,c). The corresponding Au NPs deposited onto the ZnO NT arrays (Figure 2d–f) possess similar morphology. On the top surface of the analyzed nanotubes, tiny objects can be distinguished. Figure S1 (Supporting information) shows the particle size distribution (in the form of histograms) calculated for the Au island films deposited on glass with a mass thickness of 5 nm (Au NPs-5), 2.5 nm (Au NPs-2.5), and 1 nm (Au NPs-1). The size of Au nanoparticles decreases, and the particle size distribution becomes much narrower as the Au island film mass thickness is reduced from 5 to 1 nm.

The morphology of NPs forming Ag island film is similar to that of the Au island film (Figure 3). The Ag NPs deposited onto glass are shown in images (a–c) and (g–i), and the corresponding Ag NPs deposited on top of the ZnO NTs are presented in images (d–f) and (j–l). In Figure S2 (Supporting Information), the particle size distribution for the Ag island films with a mass thickness of 6.5 nm (Ag NPs-6.5), 5 nm (Ag NPs-5), 2.5 nm (Au NPs-2.5), 2 nm (Ag NPs-2), 1.5 nm (Ag NPs-1.5), and 1 nm (Ag NPs-1) is demonstrated in the form of histograms. As in the case of the Au island film, the size of Ag NPs decreases and the particle size distribution becomes narrower as the mass thickness of the Ag film decreases. It can

https://doi.org/10.1021/acsomega.3c08253
ACS Omega 2024, 9, 1670–1682

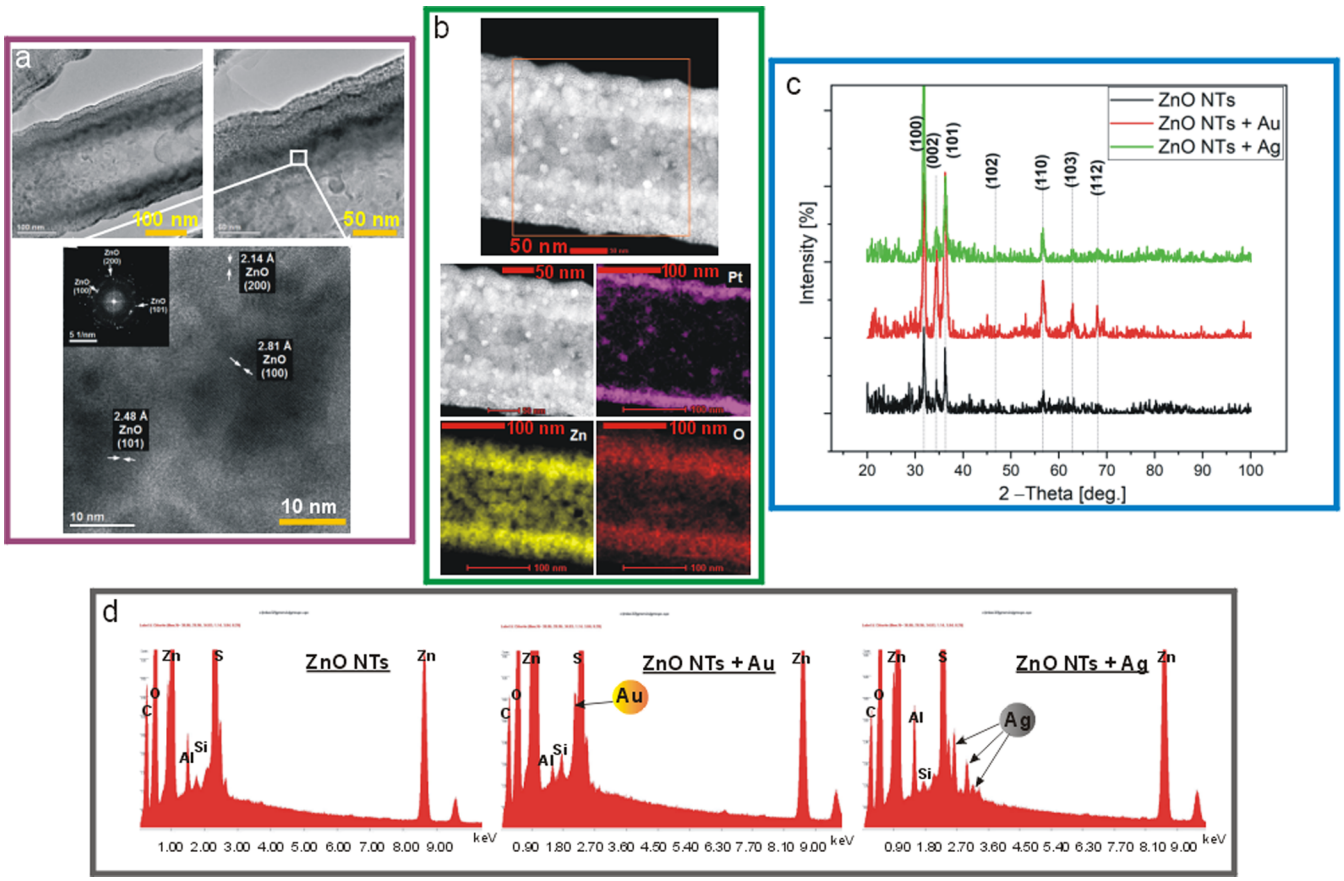

Figure 4. HR-TEM images together with FFT analysis of a single ZnO nanotube (a), STEM-HAADF images along with EDX mapping (Pt comes from the protective layer used to make the TEM lamella) of a single ZnO nanotube (b), XRD of the ZnO NTs before and after Au and Ag island film depositions (films with a 5 nm mass thickness were used in the analysis) (c), and EDS spectra of ZnO NTs before and after Au and Ag island film depositions (films with a 5 nm mass thickness were used in the analysis) (d).

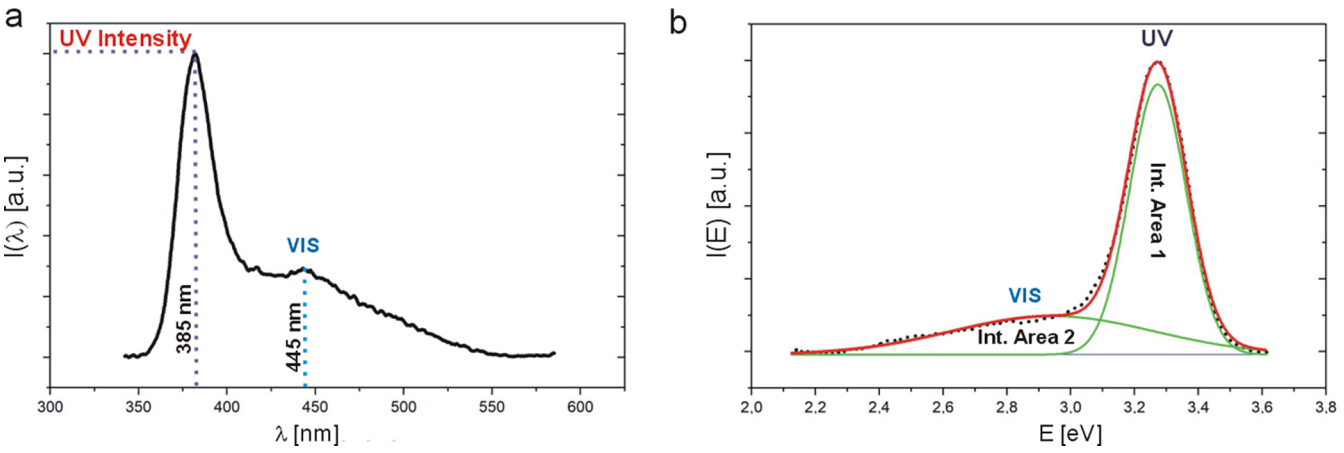

Figure 5. Photoluminescence (PL) spectrum of exemplary ZnO NT arrays (black dotted line) (a), the equivalent spectrum in energy (E) scale (black dotted line), with the fitted curve (red line) resulting from the deconvolution of the experimental spectrum by the Gaussian functions with indicated areas under the UV and VIS peaks used to calculate F_2 factor (b).

also be seen that the number of the Ag NPs with the smallest size range ([0, 50] nm^2) increases as the Ag mass thickness is reduced. Additionally, the filling factor, which translates inversely into the distance between the nanoparticles (the smaller the filling factor, the larger are the spaces between the nanoparticles), shows a clear decreasing tendency with decreasing the mass thickness of both Au and Ag metals (see Figure S3 in the Supporting Information).

Based on FFT analysis of the HR-TEM image of a single ZnO nanotube, the reflections from the following crystallographic planes were identified: (100), (101), and (200), which can be assigned to a polycrystalline ZnO with the hexagonal wurtzite structure (Figure 4a). EDX mapping demonstrates a ZnO nanotube with a uniform wall thickness of around 60 nm and an external diameter (corresponding to the pore diameter in the PAA template) of ca. 200 nm (Figure 4b). XRD patterns

https://doi.org/10.1021/acsomega.3c08253
ACS Omega 2024, 9, 1670−1682

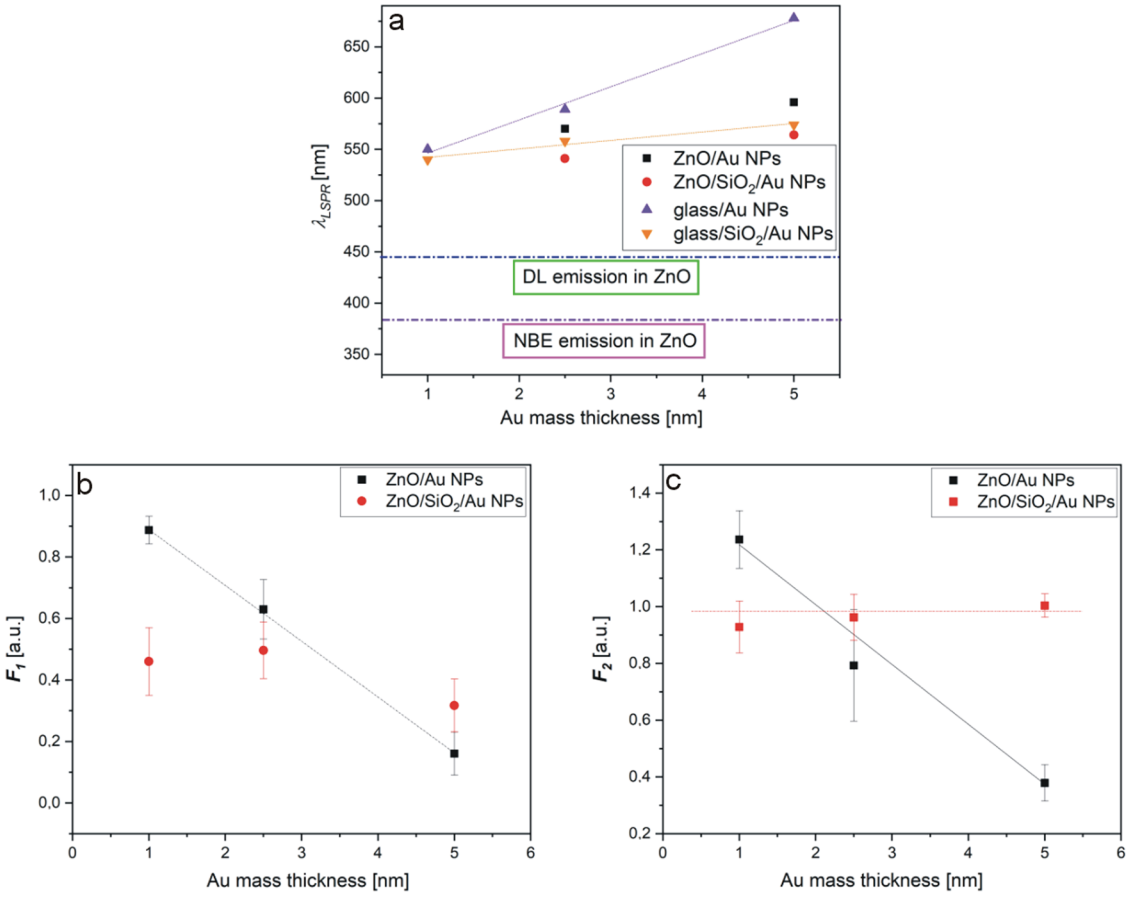

Figure 6. Plasmonic resonance (λ_{LSPR}) as a function of the Au island film mass thickness (a); F_1 (b) and F_2 (c) factors as a function of Au mass thickness (particle size distribution for the Au island films with a mass thickness of 5 nm (Au NPs-5), 2.5 nm (Au NPs-2.5), and 1 nm (Au NPs-1), respectively, is shown in Figure S1).

confirmed a polycrystalline, hexagonal wurtzite structure form of ZnO (PDF Card 00-005-0664), with the reflection peaks from the following crystallographic planes: (100), (002), (101), (102), (110), (103), and (112) (Figure 4c). No Au nor Ag was detected in the XRD profiles, most probably owing to the insufficient amount of deposited metals present in the analyzed area. The presence of Au and Ag was, however, confirmed by EDS analysis (Figure 4d), which shows distinct peaks that can be assigned to AuM and AgL lines, respectively. Apart from these peaks, the spectra show the presence of the Zn, O, S, Si, Al, and C elements. The S and C come most probably from the optical adhesive, whereas the Si originates from the glass substrate. A trace of the Al element coming from a residual PAA template could also be observed in the analyzed samples.

Room-temperature PL spectra of ZnO nanotube arrays demonstrate two characteristic peaks centered at around 385 nm (UV) and 445 nm (VIS), which are due to near-band-edge (NBE) and defect-related (DL) emission, respectively (Figure 5). The blue emission was previously attributed to the electron transitions from zinc interstitial (Zn_i) and extended Zn_i states (ex-Zn_i) to the valence band (VB).[40,41] The photoluminescence properties of the samples before and after metallic nanoparticle deposition were analyzed by determining two parameters defined according to the following formulas

$$F_1 = \frac{\text{UV intensity after metallic layer deposition}}{\text{UV intensisty befor emetallic layer deposition}} \quad (1)$$

$$F_2 = \frac{\frac{\text{UV}}{\text{VIS}}\ \text{ratio after metallic layer deposition}}{\frac{\text{UV}}{\text{VIS}}\ \text{ratio before metalliclayer depostion}} \quad (2)$$

where

$$\text{UV/VIS ratio} = \frac{\text{int. area1}}{\text{int. area2}}.$$

The integrated area under the UV (Int. Area 1 in Figure 5b) and VIS (Int. Area 2 in Figure 5b) peaks was obtained by deconvolution of the overlapping peaks in the PL spectrum using the Gaussian function (Figure 5b). F_1 refers, therefore, to the change of the UV peak intensity regardless of the VIS luminescence variation, whereas F_2 gives information about the behavior of the UV peak dependent on the changes in the VIS band, and $F_2 > 1$ means the increase of UV emission in the expense of the VIS emission ($F_2 < 1$ signifies in general the increase of VIS luminescence).

Transmittance spectra were collected to identify the absorption band corresponding to the localized surface plasmon resonance (LSPR) excitation at the metallic NPs (see Figures S4 and S7 in the Supporting Information). The LSPR is observed as a transmittance dip resulting from the absorption and scattering of the incident light of wavelengths that correspond to a specific electron oscillation frequency at metal nanoparticles (λ_{LSPR}). The λ_{NBE} line (corresponding to NBE emission in PL) refers to the absorption of light by NBE transition in ZnO. The λ_{DL} band (clearly visible only in Figure

https://doi.org/10.1021/acsomega.3c08253
ACS Omega 2024, 9, 1670−1682

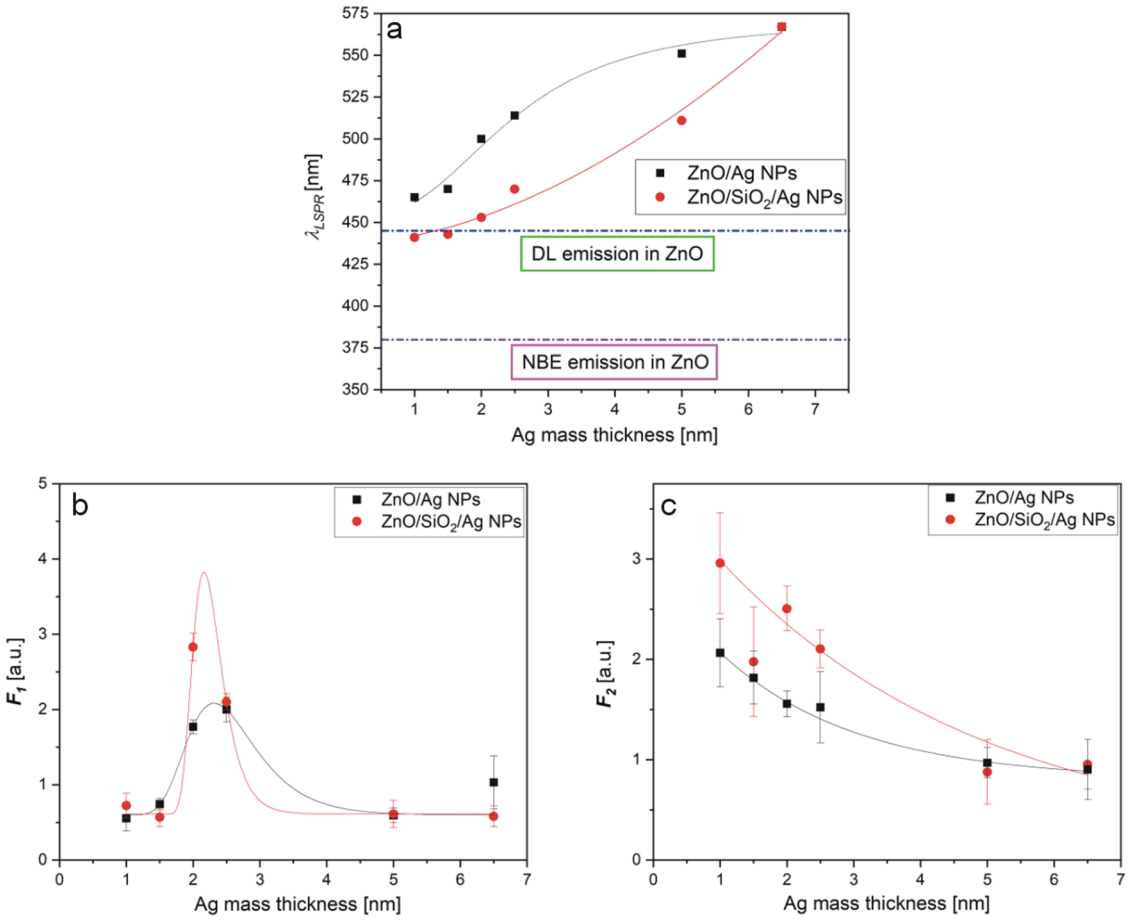

Figure 7. Plasmonic resonance (λ_{LSPR}) as a function of the Ag island film mass thickness (a); F_1 (b) and F_2 (c) factors as a function of the Ag mass thickness (particle size distribution for the Ag island-like films with a mass thickness of 6.5 nm (Ag NPs-6.5), 5 nm (Ag NPs-5), 2.5 nm (Ag NPs-2.5), 2 nm (Ag NPs-2), 1.5 nm (Ag NPs-1.5), and 1 nm (Ag NPs-1) is shown in Figure S2).

S4c) could be due to the light absorption by defect states in ZnO (corresponding to VIS emission in PL). Two types of samples were analyzed: one with metallic nanoparticles deposited directly on the ZnO surface (ZnO/Au or Ag samples) and the other with a SiO_2 spacer layer (5 nm thickness) placed between the ZnO surface and metallic NPs (ZnO/SiO_2/Au or Ag samples). The spacer is frequently used in order to avoid undesired charge transfer between the semiconductor and the metal, which may decrease the density of states in the ZnO conduction band.[42,43,28] It was also postulated that a spacer reduces coupling with nonradiative high-order LSP modes that is responsible for luminescence quenching.[44,45]

The transmittance spectra of the samples with and without the Au island film are gathered in Figure S4 (in the Supporting Information). The intensity of the LSPR extinction band drops significantly as the mass thickness and filling factor of Au nanoparticles decrease. This is probably due to the reduction of the field enhancement factor (FEF) as the size of the NPs decreases.[10] The centers of the λ_{LSPR} dips as a function of the Au mass thickness are shown in Figure 6a. The λ_{LSPR} dips in the samples ZnO/Au NPs-1 and ZnO/SiO_2/Au NPs-1 are not visible at all (Figure S4c); therefore, these points are missing in Figure 6a. The transmittance spectra were also collected for the Au island films deposited on glass without the ZnO material (sample glass/Au and glass/SiO_2/Au, respectively), where the λ_{LSPR} are well distinguished and could be well defined even for the samples with a 1 nm mass thickness (Au NPs-1). Furthermore, it can be noticed that the samples with the spacer layer (ZnO/SiO_2/Au) show stronger and better-resolved resonances compared to those without SiO_2 (ZnO/Au). This is possibly due to a better configuration between the substrate and deposited nanoparticles (e.g., lower roughness of the ZnO/SiO_2 NTs' surface as compared to bare ZnO NTs, or—in the case of metal on glass—lower wetting of glass/SiO_2 substrate by Au). The λ_{LSPR} peak shifts to shorter wavelengths with the decrease in the nanoparticle size and refractive index (RI) of the surrounding medium (RI of ZnO is higher than RI of SiO_2). Similar dependence was observed before for various metallic nanoparticles.[12,46−48] The horizontal lines in Figure 6a indicate the NBE and DL emissions in ZnO, respectively. As can be seen, the spectral positions of plasmon resonances generated by Au NPs are far away from both DL and NBE transitions in ZnO.

The PL spectra of the ZnO nanotubes before and after the Au island film deposition are shown in Figure S5 (in the Supporting Information). The analyzed areas show a distinct NBE and a weak DL emission before metal deposition. After the metal addition, the intensity of the NBE peak visibly reduces. For the samples without a SiO_2 spacer, the F_1 parameter decreases almost linearly with the increase of Au mass thickness, whereas for the samples with the SiO_2, the F_1 parameter remains more or less stable for the 1 and 2.5 nm and tends to decrease only for the 5 nm Au mass thickness Au

https://doi.org/10.1021/acsomega.3c08253
ACS Omega 2024, 9, 1670−1682

island films (Figure 6b). Since the 1 nm Au mass thickness sample is almost transparent for UV radiative emission ($F_1 \sim 1$), the behavior indicates that the spacer alone blocks quite efficiently the UV emission from ZnO: the F_1 decreases to about 0.5 for the same sample with SiO_2. The normalized PL spectra in Figure S6 (in the Supporting Information) demonstrate that upon covering the ZnO nanotube surface with the 5 nm and 2.5 Au mass thickness island films, the DL emission increases. In the latter sample (Figure S6b in the Supporting Information), apart from the VIS peak at around 445 nm, an additional peak at around 540 nm appears, which can be ascribed to transitions from ex-Zn_i levels to the zinc vacancy level (V_{Zn}).[41] As an effect of the increased DL emission, which is accompanied by the decrease in NBE emission, the F_2 in the ZnO/Au samples significantly decreases with an increase of the amount of Au mass (Figure 6c). It is worth noticing that for the corresponding samples with a SiO_2 spacer, the F_2 parameter remains stable (close to 1). This means that both UV and VIS peaks became proportionally reduced when the surface of ZnO NTs was covered with both SiO_2 and Au. For the ZnO NTs covered with the Au island film with a 1 nm mass thickness, the normalized spectra look the same (Figure S6c in the Supporting Information), meaning that the nanoparticles are probably too small to introduce any visible changes in the ZnO/Au system (F_2 parameter is around 1 for both ZnO/Au and ZnO/SiO_2/Au samples).

Ag nanoparticles usually show stronger plasmonic resonances than Au nanoparticles due to higher absorption and scattering cross sections.[8,9] In Figure S7 (the Supporting Information), transmittance spectra of the ZnO nanotubes before and after Ag deposition are presented. The dips corresponding to LSPR are much more pronounced in these samples compared with those with Au. The center positions of λ_{LSPR} were easily identified even for the samples with the 1 nm Ag mass thickness island film and are demonstrated in Figure 7a as a function of Ag mass thickness. With decreasing the mass thickness of the Ag island film, the λ_{LSPR} shifts toward the blue part of the spectrum. The shift shows a typical behavior.[48,49] However, for the Ag island films with a mass thickness < 2 nm, the shift is evidently smaller. This might be due to rather small variations in nanoparticle sizes in the 2.5−1 nm range of deposited Ag mass. As in the case of Au NPs, the resonance peaks in the ZnO/Ag NPs are positioned at longer wavelengths as compared to the λ_{LSPR} in ZnO/SiO_2/Ag NPs. This could be due to the larger RI of ZnO relative to that of SiO_2 or a different structure of the island film (different sizes of nanoparticles and distances between them) on the ZnO/SiO_2 surface. Although still far away from NBE emission, the position of the λ_{LSPR} for the smaller Ag nanoparticles is now close to (for the ZnO/Ag NPs) or overlaps with (for the ZnO/SiO_2/Ag NPs) the radiative recombination via the DL states in ZnO.

PL spectra for the ZnO NTs before and after Ag deposition are gathered in Figures S8 and S9 (the Supporting Information). It can be noticed that the photoluminescence of pristine ZnO NTs is characterized by a variable level of DL emission, which indicates different defect densities present in the material despite the same method applied to prepare the samples. However, it has to be noticed that the NaOH solution used to selectively etch the PAA template can also dissolve ZnO, although with a lower reaction rate.[50] Therefore, even if the PAA + ZnO samples were kept in the alkaline solution for the same time, ZnO could be attacked to a greater or lesser extent depending on, for example, the Al_2O_3/ZnO ratio (a small variation in the pore diameter). This, in turn, produced various numbers of defects, such as Zn_i. Regardless of the defect density, the enhancement of UV emission from ZnO NTs seems to be strongly dependent on the size of Ag NPs. After the deposition of Ag, the NBE emission is enhanced only for the Ag island film with a mass thickness of 2.5 and 2 nm (see Figure S8c,d in the Supporting Information). The other Ag island films were ineffective in intensifying UV luminescence. In Figure 7b,c, the F_1 and F_2 parameters as a function of the Ag island film mass thickness are demonstrated, respectively. A single peak extreme function was fitted to the F_1 dependence receiving the max F_1 for the mass thickness between 2 and 2.5 nm. In this nanoparticle size range, the highest F_1 of about 4 was found for the ZnO/SiO_2/Ag NPs, whereas for the ZnO/Ag NPs, the F_1 max was about 2 times smaller. Surprisingly, the F_2 dependences are entirely different. The F_2 parameter is low (close to 1) for the Ag mass thickness between 5 and 6.5 nm and starts to grow for a mass thickness of 5 nm. The highest F_2 of ca. 3 was obtained for the sample ZnO/SiO_2/Ag NPs-1. It can also be noticed that the samples with the largest F_2 are characterized by a strong VIS peak before the metal deposition, yet for these samples, the parameter $F_1 < 1$. The mismatch between F_1 and F_2 factors suggests that defect density plays a minor role in optimizing the F_1 parameter compared to the Ag NP size.

The dependence of the PL enhancement factor on the defect densities present in ZnO nanostructures was, however, observed in many previous works.[19,22,38,51] It was even suggested that strong visible DL and weak NBE emission are necessary conditions to activate the UV enhancement via LSP-DL coupling; otherwise, the opposite happens: the radiative recombination across the band gap is significantly reduced after covering the ZnO surface with metallic NPs.[51] On the other hand, it is well-known that the plasmonic properties of metallic nanoparticles depend on their size. For a certain size and particle density, absorption may become dominant over scattering leading to PL quenching.[52,53,29] Usually, the larger metallic NPs provide a larger scattering cross section in coupling surface plasmons to light to increased UV emission, whereas in the smaller ones, absorption dominates over the scattering.[16] Distance/space between the metallic NPs was also found to be an important aspect of the PL enhancement process.[16,54] Different plasmonic modes can be activated in a system depending on the distance between metallic nanoparticles.[55] Collective modes predominate when particles interact with each other, which happens when the distance between them is sufficiently small. When the spacing increases, the interaction weakens, and local plasmonic modes start to dominate. If increasing spacing (or reduction of filling factor; Figure S3) is accompanied by a decreasing size of nanoparticles, the overall processes taking place in the system may ultimately lead to stronger radiation absorption by metallic nanoparticles and the quenching of light emission from ZnO. And these are the phenomena that seem to be operative in the ZnO/Ag NP system, as indicated by the F_1 factor behavior (Figure 7b). Outside the narrow range of Ag mass thicknesses between 2 and 2.5 nm, where the UV enhancement is observed, the F_1 falls down to less than 1 (UV quenching). Likely, the size and the spacing in the island films with a 1−1.5 nm Ag mass thickness favor absorption over the scattering of light emitted from ZnO, and in this range, the UV light is quenched. Above the 2.5 nm Ag mass thickness, the size and

https://doi.org/10.1021/acsomega.3c08253
ACS Omega 2024, 9, 1670−1682

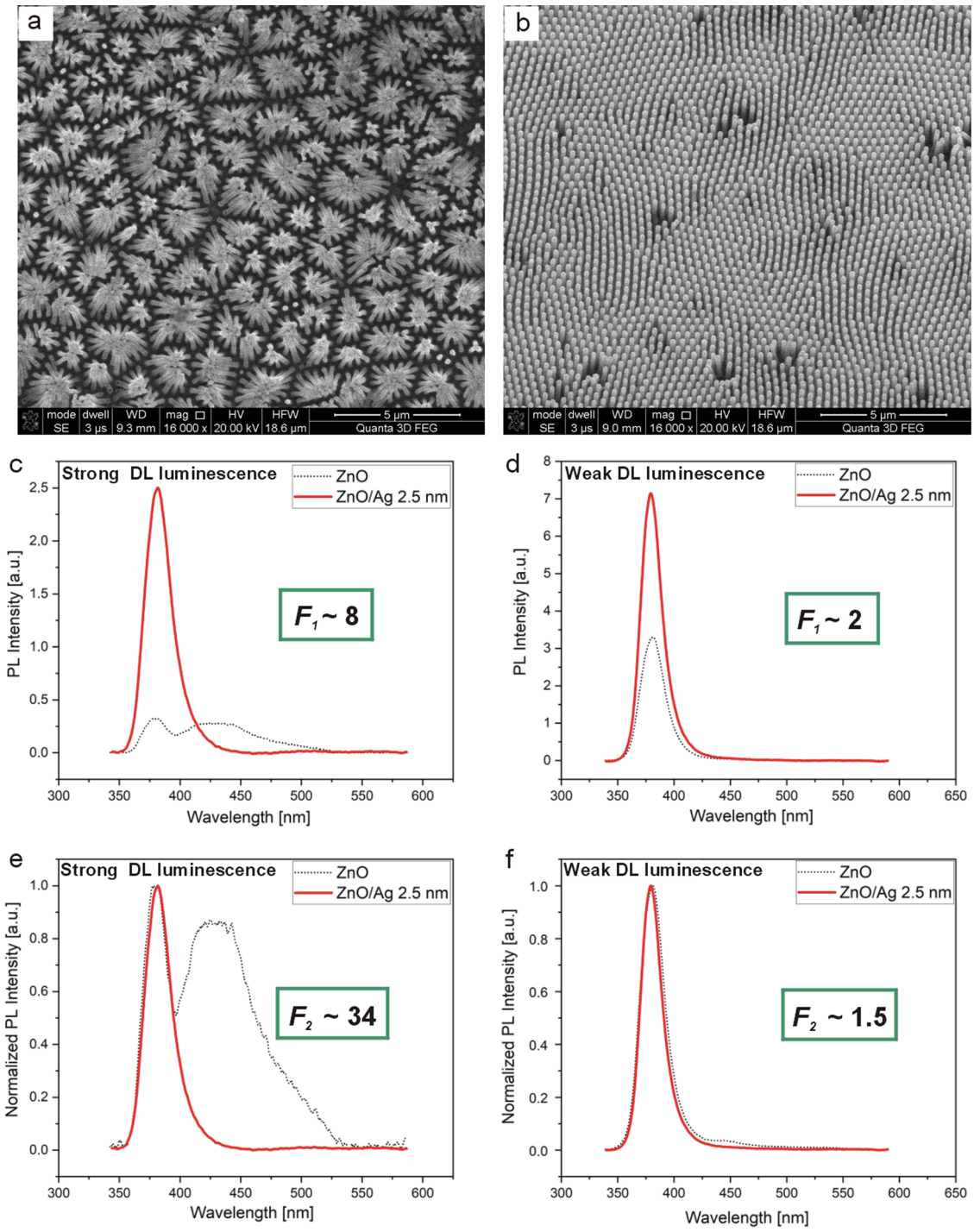

Figure 8. SEM images of the less ordered, defected ZnO NTs (a) and the well-aligned, "nondefected" ZnO NTs (b); PL (c, d) and normalized PL (e, f) spectra of the defected (c, e) and nondefected (d, f) ZnO NTs before (ZnO) and after (ZnO/Ag 2.5 nm) deposition of the Ag island film with a 2.5 nm mass thickness.

packing density of Ag NPs are simply too large (moreover, in these conditions, rather collective plasmonic modes dominate) to allow for the photon extraction, and as a result, quenching of light emitted by ZnO NTs occurs. Similar behavior of the enhancement factor on the Ag particle size was observed by Cheng et al.[30] Based on these findings, it can be assumed that optimal UV light enhancement would be achieved when the large defect density will be combined with a strong scattering efficiency of metallic nanoparticles.

To verify this assumption, an additional sample with a high defect density was prepared. To introduce a large amount of surface defects, the sample ZnO + PAA was kept in the alkaline solution for about 10 min longer than the other samples to allow for a more intensive dissolution of external nanotube walls. As an effect, the resulting ZnO NTs are geometrically much less stable (Figure 8a) in contrast to the well-arranged and well-aligned ZnO nanostructures (Figure 8b) that are characterized by a negligible defect density (very weak DL luminescence). The optical performances of both samples

https://doi.org/10.1021/acsomega.3c08253
ACS Omega 2024, 9, 1670−1682

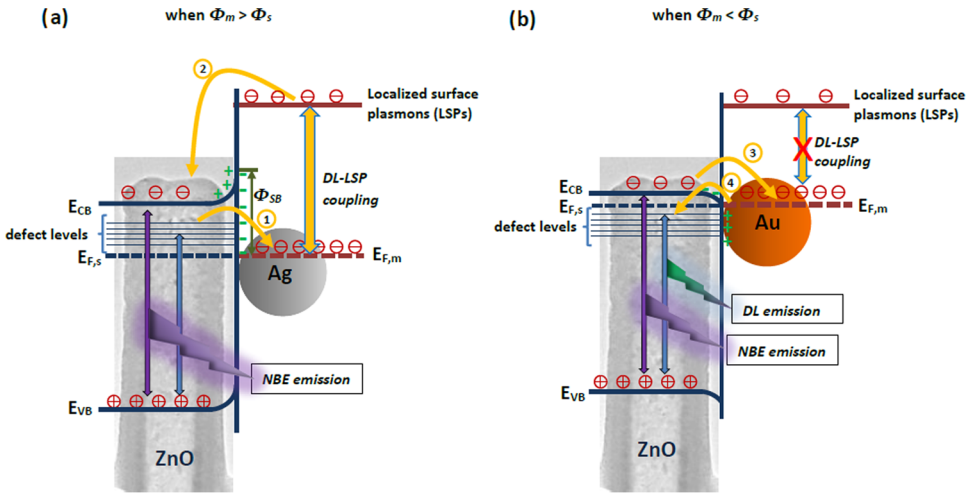

Figure 9. Energy band diagrams and charge-transfer processes at the ZnO/Ag (a) and ZnO/Au (b) interfaces (Φ_m, metal work function; Φ_s, semiconductor work function; Φ_{SB}, Schottky barrier; E_{CB}, energy of the conduction band minimum; E_{VB}, energy of the valence band maximum; $E_{F,m}$, Fermi level of the metal, $E_{F,s}$, Fermi level of the semiconductor).

before and after coating with the Ag island film with a 2.5 nm mass thickness are compared in Figure 8c–f. The PL spectrum of the highly defective ZnO NTs shows a strong DL luminescence peak of comparable intensity to the NBE peak (Figure 8c,e). The overall PL intensity is also much lower than that of well-aligned ZnO NTs, which might be due to the smaller effective number of nanoemitters per illuminated area (more nanotubes were probably detached from the substrate as a result of the longer interaction with the alkaline solution). After the coating with the Ag island film with a 2.5 nm mass thickness, the DL emission is completely suppressed, while the NBE emission becomes much stronger. A complete passivation of defects in Au-coated ZnO NRs regardless of the defect density present in the pristine ZnO NRs was also observed by Dixit et al.[38] The F_1 and F_2 parameters in the defected ZnO NTs are also much larger compared to those in the "nondefected" ZnO NTs. The F_1 is ca. 4 times, whereas the F_2 is about 23 times higher than the corresponding parameters in the "nondefected" ZnO NTs, reaching the values as high as 8 and 34, respectively. Our results demonstrate thus that even if the high defect density is not necessary for UV emission enhancement to occur, this enhancement is certainly promoted by the defects. Similar findings were presented by Prajapati et al.[56] where it was concluded that the presence of defect states may facilitate the charge transfer; however, their presence does not guarantee UV emission enhancement and strong plasmonic coupling between the semiconductor and metal. This conclusion is well mirrored in our data: despite large defect densities in the samples covered with Ag island films with 1 and 1.5 nm mass thicknesses, no UV light amplification was observed in this case. It indicates two parallel and simultaneous processes being operative in the system: one is associated with energy, and the second with charge transfer. The first process relates to the local field enhancement by surface plasmons, which increases the radiative recombination rate in ZnO. The local field enhancement can also improve the optical absorption efficiency in ZnO. In this case, the closer the λ_{LSPR} to the λ_{NBE}, the stronger is the UV enhancement. As can be seen in Figure 7a, the λ_{LSPR} is closer to λ_{DL} than to the λ_{NBE} and yet, no DL emission enhancement was observed. However, since the DL excitonic recombination originates from surface defect states in ZnO that are deactivated by both SiO_2 and Ag layers, the passivation of these defects reduces or completely suppresses the DL emission and ultimately contributes to the plasmonic enhancement of the NBE emission. The second process is promoted via the migration of photogenerated electrons in the defect levels of ZnO to the Fermi level of the metal, the excitation of the migrated electrons to higher energy levels of the metal by LSP-DL coupling, back-transfer of the hot electrons to the conduction band of ZnO, and finally the radiative recombination of the transported electrons with the holes in the valence band (VB). The second route is therefore reinforced by the electrons trapped in the defect states in ZnO: the higher the density of defect states, the larger the UV enhancement.

The processes that can occur at the ZnO/metal interface are depicted in the scheme presented in Figure 9. In general, two contacts between a metal and n-type semiconductor being in direct contact can be formed.[57] If the metal work function (Φ_m) is higher than that of the semiconductor (Φ_s), the electrons will flow from the semiconductor to the metal, causing the semiconductor Fermi level ($E_{F,s}$) to decrease until it becomes aligned with the Fermi level of the metal ($E_{F,m}$). When $\Phi_m > \Phi_s$, in an n-type semiconductor, there is a barrier formed at the metal–semiconductor interface, which is called the Schottky barrier (Φ_{SB}) (Figure 9a). The Φ_{SB} blocks the electron transfer from the metal to the conduction band (CB) in the semiconductor. In the opposite situation (when $\Phi_m < \Phi_s$), the electron will flow from the metal to the semiconductor, causing the $E_{F,m}$ to decrease and equalize with the $E_{F,s}$.[57] The metal–semiconductor contact is ohmic in the latter case (Figure 9b).

The silver tends to form the Schottky barrier in contact with ZnO,[58] and the formation of the Φ_{SB} was assumed in some works studying plasmonic enhancement of ZnO luminescence in the ZnO/Ag hybrids.[59,51,60] This type of contact is also the most probable scenario in the studied case. In this scenario, under the excitation, the electrons in the surface defect levels move to the Fermi level in Ag because their energy is higher than that of the Fermi level (process 1 in Figure 9a). When the local plasmonic modes (weakly or noninteracting particles) and scattering efficiency of nanoparticles dominate over collective modes and absorption (the case of the samples with Ag island films with 2 and 2.5 nm mass thicknesses), the

https://doi.org/10.1021/acsomega.3c08253
ACS Omega 2024, 9, 1670−1682

electrons from the Fermi level are transported to the ZnO conduction band (CB) via the DL-LSP coupling (so-called hot electrons), crossing the Schottky barrier (process 2 in Figure 9a). Subsequently, they recombine with the holes in the valence band (VB) increasing the radiative recombination ($F_1 > 1$). In this case, the larger the defect density in ZnO, the more efficient process 1 and the stronger plasmonic enhancement can be accomplished. The UV emission enhancement also occurs due to the energy transfer. The LSP-mediated local electromagnetic field generated at the metal site radiatively contributes to the local generation of electron−hole pairs in the semiconductor. The latter process does not require direct contact between the metal and the semiconductor and is governed by the energy match between the energy of excitonic recombination in the semiconductor to the electron oscillation energy at the metal/semiconductor interface.[8] For smaller Ag NPs, when the absorption cross section of Ag NPs prevails over the scattering cross section, only process 1 takes place, whereas the DL-LSP coupling is inactive. Consequently, the NBE (UV) emission is reduced. It should be noted that the quenching may also proceed via the nonradiative channel from ZnO to the NPs. Furthermore, when the DL-LSP coupling is inactive, the Schottky barrier effectively blocks the transfer of electrons from Ag to CB in ZnO and, as an effect, the $F_1 < 1$, whereas F_2 reaches the highest values.

In the ZnO/Au systems, the Schottky contact between Au and ZnO was frequently proposed to explain the UV emission enhancement via LSPR-mediated electron transfer from the metal Fermi level to the CB in ZnO.[13,35,38,61−63] However, in these systems, the LSPR of Au nanoparticles was tuned to the defect transition energy (green emission) in ZnO. In our system, the DL and LSP energies are decoupled, and therefore, this enhancement route was not possible. Moreover, instead of the Schottky contact, the system shows ohmic-like contact behavior. The formation of ohmic contact between ZnO and Au was found to be promoted by surface impurities (e.g., chemical contamination), subsurface native point defects, metal deposition that introduces additional near-interface contamination, or other semiconductor disruption, etc.[58,64−66] In this type of heterojunction, there is no barrier for electrons to flow from the metal to the semiconductor. Accordingly, upon excitation, the electrons in the CB in ZnO are easily transferred to the Fermi level in Au (process 3, Figure 9b). Because there is no DL-LSP coupling, NBE recombination is reduced. Moreover, assuming that the Fermi level in Au lies a bit higher than the defect levels in ZnO, part of the electrons can move back to the DL states in ZnO, increasing the excitonic recombination from the defect states (process 4, Figure 9b). As a result, the VIS emission from ZnO NTs increases after Au NP deposition (Figure S6a,b in the Supporting Information) and the F_2 factor decreases with the Au layer thickness (Figure 6c). In the ZnO/SiO_2/Au samples, the spacer efficiently blocks the back transport of electrons to the ZnO site, giving always $F_2 \sim 1$. In any case, processes 3 and 4 contribute to the overall quenching of UV emission in ZnO/Au hybrid nanostructures. It is worth noting that for the enhancement or quenching of luminescence in the ZnO/metal hybrid systems to happen, the charge-transfer processes 1−4 must be faster than the excitonic recombination from CB or via defect states in ZnO.

4. CONCLUSIONS

A comprehensive study comparing the impact of Au and Ag plasmonic metals on the luminescence performance of ZnO nanotubes is presented. The ZnO NTs were prepared by a template-assisted ALD synthesis, controlling the length, diameter, and wall thickness of the nanotubes. Metallic island films with NPs of different sizes and spacing were deposited on the top of the ZnO NT arrays by the electron beam PVD technique. Photoluminescence spectra before and after the metal deposition were analyzed using two parameters that referred to a UV band change regardless of the VIS band variation (F_1 parameter) and of the UV/vis ratio change (F_2 parameter). The F_1 and F_2 parameters, together with the monitoring of the metal plasmonic band (λ_{LSPR}) by transmittance measurements, allowed us to unravel a specific role of surface defects in ZnO, the size and the distance between the NPs, and the strength of plasmonic coupling in the processes occurring at the ZnO/metal interfaces. The enhancement of UV emission was observed only in the ZnO/Ag system. The plasmonic enhancement in this system proceeds via the DL-LSP coupling, involving both energy and charge transfers between the metal and the semiconductor. However, the coupling is not sufficient for the UV enhancement to occur. The metal size and spacing must be properly tuned in order to obtain larger scattering over the absorption contribution to the overall extinction cross section. In this case, the UV light can be further enhanced by the efficient transport of electrons from the defect levels in ZnO to the metal. These electrons are then transferred to the conduction band in ZnO via the DL-LSP coupling and recombine radiatively with holes in the ZnO valence band. As a result of this process, F_1 and F_2 factors as high as 8 and 34, respectively, could be obtained in the ZnO NTs characterized by strong DL emission before the Ag island film deposition. In contrast to that, the Au island films caused the quenching of the UV emission, which was ascribed to the uncoupling between the DL and LSP energies and a possible formation of the ohmic contact between the metal and the ZnO.

■ ASSOCIATED CONTENT

Supporting Information

The Supporting Information is available free of charge at https://pubs.acs.org/doi/10.1021/acsomega.3c08253.

Nanoparticle size distributions (histograms) for Au (Figure S1) and Ag (Figure S2) island-like films deposited on glass; filling factor as a function of Au and Ag mass thicknesses (Figure S3); transmittance spectra of the Au (Figure S4) and Ag (Figure S7) NPs deposited on glass and ZnO NTs, with and without a SiO_2 spacer; and PL and normalized PL spectra of ZnO NTs before and after PVD deposition of Au (Figures S5 and S6) and Ag (Figures S8 and S9) NPs, with and without a SiO_2 spacer (PDF)

■ AUTHOR INFORMATION

Corresponding Author

Małgorzata Norek − *Institute of Materials Science and Engineering, Faculty of Advanced Technologies and Chemistry, Military University of Technology, 00-908 Warsaw, Poland;* orcid.org/0000-0002-0460-486X; Email: malgorzata.norek@wat.edu.pl

https://doi.org/10.1021/acsomega.3c08253
ACS Omega 2024, 9, 1670−1682

Authors

Maksymilian Włodarski − *Institute of Optoelectronics, Military University of Technology, 00-908 Warsaw, Poland*

Michał P. Nowak − *Institute of Optoelectronics, Military University of Technology, 00-908 Warsaw, Poland*

Matti Putkonen − *Department of Chemistry, University of Helsinki, FI-00014 Helsinki, Finland;* orcid.org/0000-0002-4166-2890

Piotr Nyga − *Institute of Optoelectronics, Military University of Technology, 00-908 Warsaw, Poland;* orcid.org/0000-0002-7591-7142

Complete contact information is available at: https://pubs.acs.org/10.1021/acsomega.3c08253

Author Contributions

M.W.: methodology, investigation, data curation, and writing—review and editing. M.P.N.: methodology, investigation, and data curation. M.P.: methodology, investigation, data curation, and writing—review and editing. P.N.: methodology, data curation, and writing—review and editing. M.N.: conceptualization, methodology, investigation, data curation, visualization, writing—original draft, writing—review and editing, funding acquisition, and supervision.

Notes

The authors declare no competing financial interest.

■ ACKNOWLEDGMENTS

The research was financed by the National Science Centre, Poland (UMO-2020/37/B/ST5/01674). M.P. acknowledges funding from the Academy of Finland by the profiling action on Matter and Materials (grant no. 318913). This work utilized ALD Center Finland Research Infrastructure. The authors thank dr inż. Tomasz Durejko for his help in XRD measurements.

■ REFERENCES

(1) Janotti, A.; Van De Walle, C. G. Fundamentals of Zinc Oxide as a Semiconductor. *Rep. Prog. Phys.* **2009**, *72* (12), 126501 DOI: 10.1088/0034-4885/72/12/126501.

(2) Djurišić, A.; Ng, A. M. C.; Chen, X. Y. ZnO Nanostructures for Optoelectronics: Material Properties and Device Applications. *Prog. Quantum Electron.* **2010**, *34* (4), 191−259.

(3) Djurišić, A.; Leung, Y. H. Optical Properties of ZnO Nanostructures. *Small* **2006**, *2* (8−9), 944−961.

(4) Norek, M. Approaches to Enhance UV Light Emission in ZnO Nanomaterials. *Curr. Appl. Phys.* **2019**, *19* (8), 867−883.

(5) Juan, M. L.; Righini, M.; Quidant, R. Plasmon Nano-Optical Tweezers. *Nat. Photonics* **2011**, *5* (6), 349−356.

(6) Chettiar, U. K.; Nyga, P.; Thoreson, M. D.; Kildishev, A. V.; Drachev, V. P.; Shalaev, V. M. FDTD Modeling of Realistic Semicontinuous Metal Films. *Appl. Phys. B* **2010**, *100* (1), 159−168.

(7) Sarychev, A. K.; Shalaev, V. M. Electromagnetic Field Fluctuations and Optical Nonlinearities in Metal-Dielectric Composites. *Phys. Rep.* **2000**, *335* (6), 275−371.

(8) Okamoto, K. Surface Plasmon Enhanced Solid-State Light-Emitting Devices. In *Nanoscale Photonics and Optoelectronics*; Springer New York, 2010; pp 27−46 DOI: 10.1007/978-1-4419-7587-4_2.

(9) Nakamura, T. Enhancement of Visible-Luminescence Saturation Intensity by Surface Plasmons in Ag/ZnO Films. *Phys. Rev. Appl.* **2016**, *6* (4), No. 044009, DOI: 10.1103/PhysRevApplied.6.044009.

(10) Shabaninezhad, M.; Ramakrishna, G. Theoretical Investigation of Plasmonic Properties of Quantum-Sized Silver Nanoparticles. *Plasmonics* **2020**, *15* (3), 783−795.

(11) Liszewska, M.; Budner, B.; Norek, M.; Jankiewicz, B. J.; Nyga, P. Revisiting Semicontinuous Silver Films as Surface-Enhanced Raman Spectroscopy Substrates. *Beilstein J. Nanotechnol.* **2019**, *10*, 1048−1055.

(12) Chen, H.; Kou, X.; Yang, Z.; Ni, W.; Wang, J. Shape- and Size-Dependent Refractive Index Sensitivity of Gold Nanoparticles. *Langmuir* **2008**, *24* (10), 5233−5237.

(13) Li, L.; Wang, C.; Han, F.; Yang, S.; Jing, W.; Jiang, Z. Largely Enhanced near Band Edge Emission of Ultrathin Zinc Oxide Nanowire/Gold Nanoparticles Composites by Surface Plasmon Resonance. *Appl. Surf. Sci.* **2018**, *433*, 1154−1157.

(14) Wang, L.; Wang, X.; Mao, S.; Wu, H.; Guo, X.; Ji, Y.; Han, X. Strongly Enhanced Ultraviolet Emission of an Au@SiO2/ZnO Plasmonic Hybrid Nanostructure. *Nanoscale* **2016**, *8* (7), 4030−4036.

(15) Mahanti, M.; Basak, D. Highly Enhanced UV Emission Due to Surface Plasmon Resonance in Ag-ZnO Nanorods. *Chem. Phys. Lett.* **2012**, *542*, 110−116.

(16) Kuiri, P. K.; Pramanik, S. Large Enhancement of UV Luminescence Emission of ZnO Nanoparticles by Coupling Excitons with Ag Surface Plasmons. *J. Appl. Phys.* **2018**, *123* (15), No. 154302.

(17) Li, G. P.; Chen, R.; Guo, D. L.; Wong, L. M.; Wang, S. J.; Sun, H. D.; Wu, T. Nanoscale Semiconductor-Insulator-Metal Core/Shell Heterostructures: Facile Synthesis and Light Emission. *Nanoscale* **2011**, *3* (8), 3170−3177.

(18) Lin, Y.; Li, J.; Xu, C.; Fan, X.; Wang, B. Localized Surface Plasmon Resonance Enhanced Ultraviolet Emission and F-P Lasing from Single ZnO Microflower. *Appl. Phys. Lett.* **2014**, *105* (14), No. 142107, DOI: 10.1063/1.4898007.

(19) Park, S.; Mun, Y.; An, S.; In Lee, W.; Lee, C. Enhanced Photoluminescence of Au-Functionalized ZnO Nanorods Annealed in a Hydrogen Atmosphere. *J. Lumin.* **2014**, *147*, 5−8.

(20) Doan, Q. K.; Nguyen, M. H.; Sai, C. D.; Pham, V. T.; Mai, H. H.; Pham, N. H.; Bach, T. C.; Nguyen, V. T.; Nguyen, T. T.; Ho, K. H.; Tran, T. H. Enhanced Optical Properties of ZnO Nanorods Decorated with Gold Nanoparticles for Self Cleaning Surface Enhanced Raman Applications. *Appl. Surf. Sci.* **2020**, *505*, No. 144593.

(21) Khan, R.; Yun, J. H.; Bae, K. Bin.; Lee, I. H. Enhanced Photoluminescence of ZnO Nanorods via Coupling with Localized Surface Plasmon of Au Nanoparticles. *J. Alloys Compd.* **2016**, *682*, 643−646.

(22) Zhang, Y.; Li, X.; Ren, X. Effects of Localized Surface Plasmons on the Photoluminescence Properties of Au-Coated ZnO Films. *Opt. Express* **2009**, *17* (11), 8735−8740.

(23) Shao, D.; Sun, H.; Yu, M.; Lian, J.; Sawyer, S. Enhanced Ultraviolet Emission from Poly(Vinyl Alcohol) ZnO Nanoparticles Using a SiO2-Au Core/Shell Structure. *Nano Lett.* **2012**, *12* (11), 5840−5844.

(24) Zhang, N.; Tang, W.; Wang, P.; Zhang, X.; Zhao, Z. In Situ Enhancement of NBE Emission of Au-ZnO Composite Nanowires by SPR. *CrystEngComm* **2013**, *15* (17), 3301−3304.

(25) Mayo, D. C.; Marvinney, C. E.; Bililign, E. S.; McBride, J. R.; Mu, R. R.; Haglund, R. F. Surface-Plasmon Mediated Photoluminescence from Ag-Coated ZnO/MgO Core-Shell Nanowires. *Thin Solid Films* **2014**, *553*, 132−137.

(26) Lu, H.; Xu, X.; Lu, L.; Gong, M.; Liu, Y. Photoluminescence Enhancement of ZnO Microrods Coated with Ag Nanoparticles. *J. Phys.: Condens. Matter* **2008**, *20* (47), No. 472202.

(27) Norek, M.; Łuka, G.; Godlewski, M.; Płociński, T.; Michalska-Domańska, M.; Stępniowski, W. J. Plasmonic Enhancement of Blue Emission from ZnO Nanorods Grown on the Anodic Aluminum Oxide (AAO) Template. *Appl. Phys. A* **2013**, *111* (1), 265−271.

(28) Mahanti, M.; Basak, D. Enhanced Photoluminescence in Ag@SiO2 Core-Shell Nanoparticles Coated ZnO Nanorods. *J. Lumin.* **2014**, *154*, 535−540.

(29) Sarkar, A.; Gogurla, N.; Shivakiran Bhaktha, B. N.; Ray, S. K. Plasmonic Enhanced Optical Characteristics of Ag Nanostructured ZnO Thin Films. *Mater. Res. Express* **2016**, *3* (4), No. 046403, DOI: 10.1088/2053-1591/3/4/046403.

(30) Cheng, P.; Li, D.; Yuan, Z.; Chen, P.; Yang, D. Enhancement of ZnO Light Emission via Coupling with Localized Surface Plasmon of

Ag Island Film. *Appl. Phys. Lett.* **2008**, *92* (4), No. 041119, DOI: 10.1063/1.2839404.
(31) Zhou, X.; Jiang, M.; Wu, Y.; Ma, K.; Liu, Y.; Wan, P.; Kan, C.; Shi, D. Hybrid Quadrupole Plasmon Induced Spectrally Pure Ultraviolet Emission from a Single AgNPs@ZnO:Ga Microwire Based Heterojunction Diode. *Nanoscale Adv.* **2020**, *2* (3), 1340−1351.
(32) Fiedler, S.; Lee Cheong Lem, L. O.; Ton-That, C.; Hoffmann, A.; Phillips, M. R. Enhancement of the UV Emission from Gold/ZnO Nanorods Exhibiting No Green Luminescence. *Opt. Mater. Express* **2020**, *10* (6), 1476.
(33) Zhou, X. D.; Xiao, X. H.; Xu, J. X.; Cai, G. X.; Ren, F.; Jiang, C. Z. Mechanism of the Enhancement and Quenching of ZnO Photoluminescence by ZnO-Ag Coupling. *Europhys. Lett.* **2011**, *93* (5), No. 57009, DOI: 10.1209/0295-5075/93/57009.
(34) Huo, C.; Jiang, H.; Lu, Y.; Han, S.; Jia, F.; Zeng, Y.; Cao, P.; Liu, W.; Wangying, X.; Liu, X.; Zhu, D. Tunable Photoluminescence Effect from ZnO Films of Ag-Decorated Localized Surface Plasmon Resonance by Varying Positions of Ag Nanoparticles. *Mater. Res. Bull.* **2019**, *111*, 17−23.
(35) Villani, M.; Rossi, F.; Calestani, D.; Salviati, G.; Fabbri, F. Evaluating the Plasmon-Exciton Interaction in ZnO Tetrapods Coupled with Gold Nanostructures by Nanoscale Cathodoluminescence. *Nano Express* **2021**, *2* (1), No. 014004.
(36) Ruiz Peralta, M. D. L.; Pal, U.; Zeferino, R. S. Photoluminescence (PL) Quenching and Enhanced Photocatalytic Activity of Au-Decorated ZnO Nanorods Fabricated through Microwave-Assisted Chemical Synthesis. *ACS Appl. Mater. Interfaces* **2012**, *4* (9), 4807−4816.
(37) Sieber, B.; Addad, A.; Szunerits, S.; Boukherroub, R. Stacking Faults-Induced Quenching of the UV Luminescence in ZnO. *J. Phys. Chem. Lett.* **2010**, *1* (20), 3033−3038.
(38) Dixit, T.; Palani, I. A.; Singh, V. Selective Tuning of Enhancement in near Band Edge Emission in Hydrothermally Grown ZnO Nanorods Coated with Gold. *J. Lumin.* **2016**, *170*, 180−186.
(39) Purahmad, M.; Stroscio, M. A.; Dutta, M. Strong Enhancement of Near-Band-Edge Photoluminescence of ZnO Nanowires Decorated with Sputtered Metallic Nanoparticles. *J. Electron. Mater.* **2014**, *43* (3), 740−745.
(40) Zeng, H.; Duan, G.; Li, Y.; Yang, S.; Xu, X.; Cai, W. Blue Luminescence of ZnO Nanoparticles Based on Non-Equilibrium Processes: Defect Origins and Emission Controls. *Adv. Funct. Mater.* **2010**, *20* (4), 561−572.
(41) Shen, H.; Shi, X.; Wang, Z.; Hou, Z.; Xu, C.; Duan, L.; Zhao, X.; Wu, H. Defects Control and Origins of Blue and Green Emissions in Sol-Gel ZnO Thin Films. *Vacuum* **2022**, *202*, No. 111201.
(42) Mahanti, M.; Basak, D. Enhanced Emission Properties of Au/SiO2/ZnO Nanorod Layered Structure: Effect of SiO2 Spacer Layer and Role of Interfacial Charge Transfer. *RSC Adv.* **2014**, *4* (30), 15466−15473.
(43) Zhao, J.; Cui, S.; Zhang, X.; Li, W. Significantly Enhanced UV Luminescence by Plasmonic Metal on ZnO Nanorods Patterned by Screen-Printing. *Nanotechnology* **2018**, *29* (35), No. 355703.
(44) Liu, M.; Chen, R.; Adamo, G.; MacDonald, K. F.; Sie, E. J.; Sum, T. C.; Zheludev, N. I.; Sun, H.; Fan, H. J. Tuning the Influence of Metal Nanoparticles on ZnO Photoluminescence by Atomic-Layer-Deposited Dielectric Spacer. *Nanophotonics* **2013**, *2* (2), 153−160.
(45) Ko, C. T.; Han, Y. Y.; Chen, C. H.; Shieh, J.; Chen, M. J. Enormous Plasmonic Enhancement and Suppressed Quenching of Luminescence from Nanoscale ZnO Films by Uniformly Dispersed Atomic-Layer-Deposited Platinum with Optimized Spacer Thickness. *J. Phys. Chem. C* **2013**, *117* (49), 26204−26212.
(46) Katyal, J.; Soni, R. K. Size- and Shape-Dependent Plasmonic Properties of Aluminum Nanoparticles for Nanosensing Applications. *J. Mod. Opt.* **2013**, *60* (20), 1717−1728.
(47) Chan, G. H.; Zhao, J.; Schatz, G. C.; Duyne, R. P. V. Localized Surface Plasmon Resonance Spectroscopy of Triangular Aluminum Nanoparticles. *J. Phys. Chem. C* **2008**, *112* (36), 13958−13963.
(48) Amirjani, A.; Firouzi, F.; Haghshenas, D. F. Predicting the Size of Silver Nanoparticles from Their Optical Properties. *Plasmonics* **2020**, *15* (4), 1077−1082.
(49) Huang, T.; Xu, X. H. N. Synthesis and Characterization of Tunable Rainbow Colored Colloidal Silver Nanoparticles Using Single-Nanoparticle Plasmonic Microscopy and Spectroscopy. *J. Mater. Chem.* **2010**, *20* (44), 9867−9876.
(50) Sun, K. G.; Li, Y. V.; Saint John, D. B.; Jackson, T. N. PH-Controlled Selective Etching of Al2O3 over ZnO. *ACS Appl. Mater. Interfaces* **2014**, *6* (10), 7028−7031.
(51) Li, L.; Yao, C.; Ding, B.; Xu, N.; Sun, J.; Wu, J. Influence of Metal Covering with a Schottky or Ohmic Contact on the Emission Properties of ZnO Nanorod Arrays. *J. Lumin.* **2023**, *257*, No. 119729.
(52) Niu, B. J.; Wu, L. L.; Tang, W.; Zhang, X. T.; Meng, Q. G. Enhancement of Near-Band Edge Emission of Au/ZnO Composite Nanobelts by Surface Plasmon Resonance. *CrystEngComm* **2011**, *13* (11), 3678−3681.
(53) Xia, Y.; Halas, N. J. Shape-controlled synthesis and surface plasmonic properties of metallic nanostructures. *MRS Bull.* **2005**, *30*, 338−348, DOI: 10.1557/mrs2005.96.
(54) Wang, X.; Ye, Q.; Bai, L. H.; Su, X.; Wang, T. T.; Peng, T. W.; Zhai, X. Q.; Huo, Y.; Wu, H.; Liu, C.; Bu, Y. Y.; Ma, X. H.; Hao, Y.; Ao, J. P. Enhanced UV Emission from ZnO on Silver Nanoparticle Arrays by the Surface Plasmon Resonance Effect. *Nanoscale Res. Lett.* **2021**, *16* (1), No. 8, DOI: 10.1186/s11671-020-03470-2.
(55) Krishchenko, I. M.; Manoilov, G.; Kravchenko, S. A.; Snopok, B. A. Resonant Optical Phenomena in Heterogeneous Plasmon Nanostructures of Noble Metals: A Review. *Theor. Exp. Chem.* **2020**, *56* (2), 67−110.
(56) Prajapati, K. N.; Johns, B.; Bandopadhyay, K.; Silva, S. R. P.; Mitra, J. Interaction of ZnO Nanorods with Plasmonic Metal Nanoparticles and Semiconductor Quantum Dots. *J. Chem. Phys.* **2020**, *152* (6), No. 064704, DOI: 10.1063/1.5138944.
(57) Zhang, Z.; Yates, J. T. Band Bending in Semiconductors: Chemical and Physical Consequences at Surfaces and Interfaces. *Chem. Rev.* **2012**, *112* (10), 5520−5551.
(58) Brillson, L. J.; Lu, Y. ZnO Schottky Barriers and Ohmic Contacts. *J. Appl. Phys.* **2011**, *109* (12), No. 121301.
(59) Abbass, A. E.; Swart, H. C.; Kroon, R. E. Non-Plasmonic Enhancement of the near Band Edge Luminescence from ZnO Using Ag Nanoparticles. *J. Lumin.* **2017**, *182*, 263−267.
(60) Lai, C. W.; An, J.; Ong, H. C. Surface-Plasmon-Mediated Emission from Metal-Capped ZnO Thin Films. *Appl. Phys. Lett.* **2005**, *86* (25), No. 251105.
(61) Qin, F. F.; Xu, C. X.; Zhu, Q. X.; Lu, J. F.; You, D. T.; Xu, W.; Zhu, Z.; Manohari, A. G.; Chen, F. Extra Green Light Induced ZnO Ultraviolet Lasing Enhancement Assisted by Au Surface Plasmons. *Nanoscale* **2018**, *10* (2), 623−627.
(62) Shahine, I.; Jradi, S.; Beydoun, N.; Gaumet, J. J.; Akil, S. Plasmon-Enhanced Photoluminescence and Photocatalysis Reactions in Metal-Semiconductor Nanomaterials: UV-Generated Hot Electron in Gold-Zinc Oxide. *ChemPhotoChem* **2020**, *4* (3), 181−194.
(63) Do, T. A. T.; Ho, T. G.; Bui, T. H.; Pham, Q. N.; Giang, H. T.; Do, T. T.; Nguyen, D. Van.; Tran, D. L. Surface-Plasmon-Enhanced Ultraviolet Emission of Au-Decorated ZnO Structures for Gas Sensing and Photocatalytic Devices. *Beilstein J. Nanotechnol.* **2018**, *9* (1), 771−779.
(64) Su, L.; Guan, Z.; Liu, Q.; Zhu, Y. Ohmic-Schottky Conversion of ZnO/Metal Contact Modulated by a Plasma Surface Treatment Method. *Res. Mater.* **2022**, *15*, No. 100290.
(65) Mosbacker, H. L.; Zgrabik, C.; Hetzer, M. J.; Swain, A.; Look, D. C.; Cantwell, G.; Zhang, J.; Song, J. J.; Brillson, L. J. Thermally Driven Defect Formation and Blocking Layers at Metal-ZnO Interfaces. *Appl. Phys. Lett.* **2007**, *91* (7), No. 072102, DOI: 10.1063/1.2772664.
(66) Gu, Q. L.; Cheung, C. K.; Ling, C. C.; Ng, A. M. C.; Djurišić, A. B.; Lu, L. W.; Chen, X. D.; Fung, S.; Beling, C. D.; Ong, H. C. Au/n-ZnO Rectifying Contact Fabricated with Hydrogen Peroxide Pretreatment. *J. Appl. Phys.* **2008**, *103* (9), No. 093706.